

Effective technique to analyze transmission line conductors under high intensity winds

Haitham Aboshosha^a and Ashraf El Damatty^{*}

Department of Civil and Environmental Engineering, Western University, London, Ontario, Canada

(Received July 10, 2013, Revised October 1, 2013, Accepted October 28, 2013)

Abstract. An effective numerical technique to calculate the reactions of a multi-spanned transmission line conductor system, under arbitrary loads varying along the spans, is developed. Such variable loads are generated by High Intensity Wind (HIW) events in the form of tornadoes and downburst. First, a semi-closed form solution is derived to obtain the displacements and the reactions at the ends of each conductor span. The solution accounts for the nonlinearity of the system and the flexibility of the insulators. Second, a numerical scheme to solve the derived closed-form solution is proposed. Two conductor systems are analyzed under loads resulting from HIW events for validation of the proposed technique. Non-linear Finite Element Analyses (FEA) are also conducted for the same two systems. The responses resulting from the technique are shown to be in a very good agreement with those resulting from the FEA, which confirms the technique accuracy. Meanwhile, the semi-closed form technique shows superior efficiency in terms of the required computational time. The saving in computational time has a great advantage in predicting the response of the conductors under HIW events, since this requires a large number of analyses to cover different potential locations and sizes of those localized events.

Keywords: High Intensity Wind (HIW); conductors; cable; finite element; numerical technique; downburst; tornado

1. Introduction

Transmission lines are used to carry electricity from the source of production to the consumers. They consist of towers, conductors, insulators and ground wires. Conductors, which are responsible for transmitting the electricity, are supported by the towers using insulators. Ground wires, which are usually smaller than the conductors, transmit the electrical charges in the case of lightning to the ground. Because they are usually located in rural areas, a failure in transmission lines requires a long time to repair. Such failures may cause consumer long outage time, which can lead to substantial economical losses in addition to the repairing costs. By reviewing many cases of weather-related transmission line failures around the world, it is evident that most of the failures are results of High Intensity Winds (HIW) in the form of downburst or tornados. For example, Manitoba Hydro (1996) company, Canada, reported a failure of 19 transmission towers due to a downburst. Li (2000) reported that more than 90% of transmission line failures in Australia

^{*}Corresponding author, Professor, E-mail: damatty@uwo.ca

^a Ph. D. Candidate, E-mail haboshos@uwo.ca

resulted from downburst events that are usually associated with thunderstorms. A downburst is a strong downdraft that induces an outburst of damaging winds near the ground as described by Fujita (1999). A tornado, by contrast, is a short-lived localized set of surface vortex flows extending from the clouds to the earth and associated with strong uplift.

Savory *et al.* (2001) studied the failure of a transmission tower under both downburst and tornado wind fields. By neglecting the forces acting on the conductors, failures were only predicted in the case of tornadoes, while no failure was shown to be associated with downbursts. The failure study performed by Shehata *et al.* (2008) predicted three different failure modes for the towers while being subjected to downbursts. Due to the localized nature of a downburst, wind forces acting on the conductor spans on either sides of a tower can be significantly different. This can lead to a variation in the longitudinal tensile forces acting on the two spans. The difference between those two forces can lead to a large longitudinal load transmitted to the tower cross arms, causing out-of-plane bending in this region. The study conducted by Shehata *et al.* (2008) revealed that the most critical failure mode resulted from this longitudinal load transmitted from the conductors to the towers. The recent failure study performed by El Damatty and Aboshosha (2012) indicated a similar failure. Aboshosha and El Damatty (2013) conducted a parametric study to calculate the transmitted longitudinal and transverse loads from the conductor to the towers when conductors are subjected to different downbursts. The study showed that the longitudinal load can exceed 60% of the transverse load, and therefore, cannot be ignored. The above studies emphasize the importance of designing transmission towers to withstand the downburst loads acting on the conductors.

In previous studies aiming to describe the behaviour and/or the failure modes of transmission line structures under HIW, Finite Element Analysis (FEA) was utilized to calculate the conductor reactions. In the work done by Shehata and El Damatty (2007), conductors and ground wires were modeled using the 2D-Non-linear Consistent Beam Element developed by Koziey and Mirza (1994). The analysis was performed in two directions separately: horizontally to obtain the response under the radial downburst velocities, and vertically to account for the vertical downburst velocities and the conductor's own weight. The two-dimensional element was acceptable for downbursts as their associated velocities in the horizontal direction are much higher than those in the vertical direction, and thus decoupling between the two directions can be justified. On the other hand, tornadoes have comparable velocities in all three directions. As such, Hamada and El Damatty (2011) used a three-dimensional non-linear Cable Element to model the conductors. Due to the high level of flexibility of conductors and significant nonlinear behaviour, their analysis using FEA is a time-consuming exercise. Due to the localized nature of HIW, the analysis of TL under such events needs to be repeated many times by considering different sizes and various locations for the events, as reported by Shehata and El Damatty, Hamada and El Damatty (2011) and Darwish *et al.* (2010). As such, it is important to develop a time-efficient technique to analyze multi-span conductors under both transverse and vertical loads that vary along the conductor spans.

Irvine (1981) derived a closed-form solution for the reactions of a single-spanned conductor when the loading can be fitted with a 3rd degree polynomial. Also, Yu *et al.* (1995) derived an exact solution to calculate the reactions for a single-spanned conductor subjected to high concentrated loads. The flexibility of the insulators was neglected in both solutions. As indicated by Darwish *et al.* (2010), the insulator flexibility is important in quantifying the amount of forces carried by the towers. Winkelman (1959) developed the concept of rolling span, which accounts for the insulator flexibility. However, it is based on neglecting the differences between the

conductors' tensile forces in the adjacent spans, and therefore, no longitudinal reactions are transmitted from the conductors to the supporting towers. That is not true for the case of HIW which causes unbalanced loading on the conductor spans adjacent to a tower. Ahmadi-Kashani and Bell (1988) and Wie *et al.* (1999) developed cable elements able to simulate a whole span based on the analytical solution of elastic catenary. Such elements have the big advantage of reducing the degrees of freedom, and consequently, the computational time. However, such elements can be used for uniform wind loads only, which is not the case for HIW.

2. Formulation

In this study, the multi-spanned conductor system illustrated in Fig. 1 is considered for analysis. The system has spans with length, L_x , and sag, S , under the conductor's own weight. Each span is supported by two insulators with a length, v . The insulators are assumed to be axially rigid. The system is subjected to loads in the transverse direction Y defined as $g_y(x)$ and in the vertical Z direction defined as $g_z(x)$. As a result, the conductor system will have displacements and reactions in the X , Y and Z directions.

The analysis is performed by dividing the system in to a number of elements at the conductor-insulator connecting points, which are named, $N-1$, N and $N+1$, as shown in Fig. 1. A cut on a typical conductor-insulator point ($\#N$), given by Fig. 2, shows three unknown displacement components, dx_N , dy_N and dz_N and three unknown reaction components, R_{xN} , R_{yN} and R_{zN} , in x , y and z directions, respectively. At all the connections, six unknowns exist: three reaction components and three displacement components. Therefore in order to solve for those unknowns, six equations are required at each connecting point. Three equations are derived by studying the moment equilibrium of the conductors and by equating the conductor length using two different approaches, as will be illustrated by subsections 2.1 and 2.2. The remaining three equations are derived by satisfying the equilibrium of the insulator as will be illustrated by subsection 2.3.

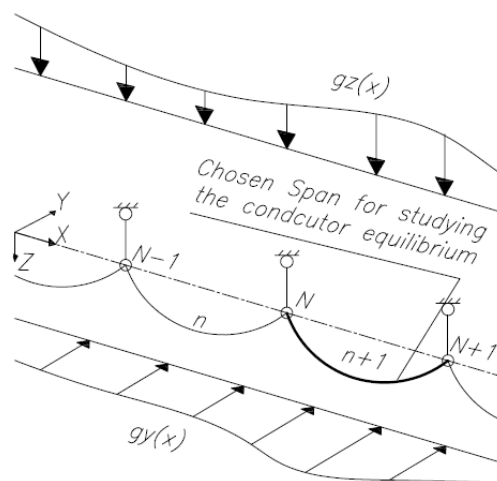


Fig. 1 The system layout

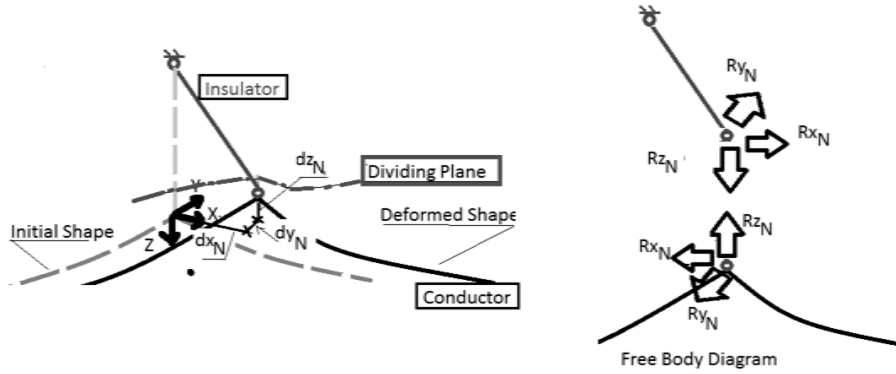


Fig. 2 Dividing the system at insulator-conductor connecting point N

2.1 Conductor transverse and vertical reactions (R_y and R_z)

Conductor equilibrium is utilized to obtain expressions for the reactions in Y and Z directions. Conductor span, $n+1$, which spans between the connecting points, N and $N+1$, and illustrated in bold in Fig. 1, is considered in the derivation below. Such a span has six end displacements d_{xN} , d_{yN} , d_{zN} , d_{xN+1} , d_{yN+1} and d_{zN+1} and five end reactions, $(R_x)_{n+1}$, $(R_y)_{n+1}$, $(R_z)_{n+1}$, $(R_y)_{n+1}$ and $(R_z)_{n+1}$, as illustrated in Fig. 3. It should be noted that since no longitudinal forces act on the conductor, the reaction, $(R_x)_{n+1}$, at the end A and that at the end B are set to be equal.

By applying the moment equilibrium at the end points, B and A, around Z and Y directions, expressions for the reactions in y direction, at the end A $(R_y)_{n+1}$ and at the end B $(R_y)_{n+1}$, and in z direction, at the end A $(R_z)_{n+1}$ and at the end B $(R_z)_{n+1}$, can be derived as indicated by Eqs. (1)-(4), respectively. Such equations depend on the first order moment induced by the external loads at point A, M_{zgyA} and M_{ygzA} , and at point B, M_{zgyB} and M_{ygzB} , which are defined by Eq. (5).

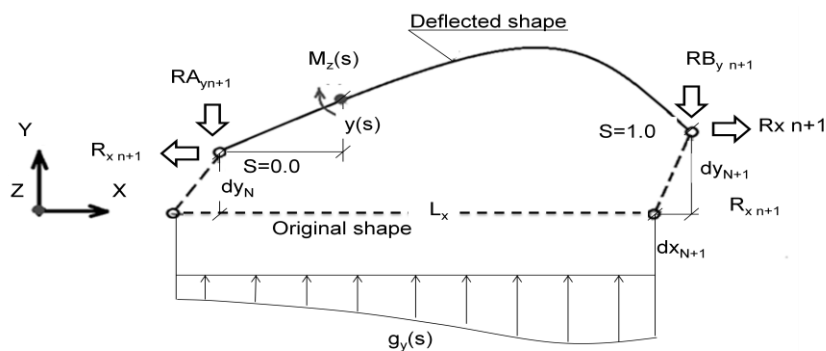


Fig. 3 Analysis of a conductor span (n+1)

$$(RA_y)_{n+1} = \frac{M_{zgyB} + (R_x)_{n+1}(dy_{n+1} - dy_n)}{L_x} \tag{1}$$

$$(RB_y)_{n+1} = \frac{M_{zgyA} - (R_x)_{n+1}(dy_{n+1} - dy_n)}{L_x} \tag{2}$$

$$(RA_z)_{n+1} = \frac{M_{ygzB} + (R_x)_{n+1}(dz_{n+1} - dz_n)}{L_x} \tag{3}$$

$$(RB_z)_{n+1} = \frac{M_{ygzA} - (R_x)_{n+1}(dz_{n+1} - dz_n)}{L_x} \tag{4}$$

$$M_{zgyB} = L_x^2 \cdot \int_{s=0}^{s=1} g_y(s) \cdot (1-s) \cdot ds \quad M_{zgyA} = L_x^2 \cdot \int_{s=0}^{s=1} g_y(s) \cdot (s) \cdot ds \tag{5}$$

$$M_{ygzB} = L_x^2 \cdot \int_{s=0}^{s=1} g_z(s) \cdot (1-s) \cdot ds \quad M_{ygzA} = L_x^2 \cdot \int_{s=0}^{s=1} g_z(s) \cdot (s) \cdot ds$$

where:

M_{igK} : The first order moment around axis i at point K induced by a loading $g_i(s)$

s: Local coordinate in the longitudinal direction =0.0 and 1.0 at the conductor start and end points

$g_y(s), g_z(s)$: Load intensity at the location s, in y and z directions, respectively.

For a connecting point, N, the reactions in Y and Z directions, R_{yN} and R_{zN} , are equal to the summation of the reactions, $(RB_y)_n$ and $(RB_z)_n$, from the end B in span N and the reactions, $(RA_y)_{n+1}$ and $(RA_z)_{n+1}$, from the end A at span N+1, as indicated by Eqs. (6) and (7), respectively. Eqs. (6) and (7) can be rewritten in a matrix notation to express the reaction vectors in y and z directions, $\{R_y\}_{Nd \times 1}$ and $\{R_z\}_{Nd \times 1}$, for N_d number of connecting points, as illustrated by Eqs. (8) and (9), respectively. Reaction vectors, $\{R_y\}_{Nd \times 1}$ and $\{R_z\}_{Nd \times 1}$, given by Eqs. (8) and (9) are the total reaction due to first and second order analyses. First order analysis assumes no displacements exist at the span ends and is represented in the reaction vectors, $\{R_y^F\}_{Nd \times 1}$ and $\{R_z^F\}_{Nd \times 1}$, which are only functions of the applied loads, g_y and g_z , respectively and defined in Appendix 1. Second order analysis accounts for displacements and their effect on the reactions. Such effect is considered by the multiplication of the stiffness matrix, $[K]_{Nd \times Nd}$ with the displacement vectors $\{dy\}$ or $\{dz\}$, as shown by Eqs. (8) and (9), respectively.

So far, transverse and vertical reactions at a general conductor-insulator node N can be calculated according to Eqs. (6) and (7). In the next subsection, 2.2, an expression for the longitudinal reaction is to be derived.

$$R_{yN} = RA_{yn+1} + RB_{yn} = \frac{M_{zgyB} + M_{zgyA} + R_x n}{L_x} - \frac{R_x n}{L_x} dy_{N-1} + \left(\frac{R_x n}{L_x} + \frac{R_x n+1}{L_x} \right) dy_N - \frac{R_x n+1}{L_x} dy_{N+1} \tag{6}$$

$$R_{zN} = RA_{zn+1} + RB_{zn} = \frac{M_{ygzBn} + M_{ygzAn+1}}{L_x} - \frac{R_{xn}}{L_x} d_{zN-1} + \left(\frac{R_{xn}}{L_x} + \frac{R_{xn+1}}{L_x} \right) d_{zN} - \frac{R_{xn+1}}{L_x} dz_{N+1} \quad (7)$$

$$\{R_y\}_{Ndx1} = \{R_y^F\}_{Ndx1} + [K]_{NdxNd} \cdot \{dy\}_{Ndx1} \quad (8)$$

$$\{R_z\}_{Ndx1} = \{R_z^F\}_{Ndx1} + [K]_{NdxNd} \cdot \{dz\}_{Ndx1} \quad (9)$$

where:

N_d : Number of conductor-insulator connecting points = number of spans+1

$\{R_y^F\}_{Ndx1}$, $\{R_z^F\}_{Ndx1}$: Vectors of y and z reactions considering no end displacements, which are defined in Appendix 1.

$[K]_{NdxNd}$: Equivalent stiffness matrix to account for the effect of the end displacement on the reactions, which is defined in Appendix 1

2.2 Conductor longitudinal reaction (R_x)

An expression for the longitudinal reaction component, R_x , is derived by evaluating the length of the deformed conductor using two approaches. The first approach is based on the axial strain of the member, as indicated by Eq. (10). The second approach is based on the length of the transverse-vertical elastic profile of the conductor. The length of an infinitesimal segment, dL , shown in Fig. 4, can be calculated as a function of the transverse slope dy/dx and the vertical slope dz/dx as indicated by Eq. (11), which can be simplified to Eq. (12). The derivatives dy/dx and dz/dx are required in the simplified integral and can be calculated by the expressions given in Eqs. (13) and (14), respectively. Such expressions are based on the assumption that no bending moment can be resisted by the conductor, and therefore, external bending moments along the deformed conductor are equal to zero. The derivatives dy/dx and dz/dx depend on the first order shearing forces, $Q_y(s)^*$ and $Q_z(s)^*$, expressed by Eqs. (15) and (16), respectively. By substituting the shearing forces in the integral presented by Eq. (12), an expression for the conductor longitudinal reaction can be derived as indicated by Eq. (17). At the conductor-insulator connecting point, N, the reaction in X direction, R_{xN} , can be calculated by subtracting the longitudinal reaction of the left span, R_{xn} , from the reaction of the right span, R_{xn+1} , as indicated by Eq. (18).

$$L = L_0 \cdot \left(1 + \frac{R_x - R_{x0}}{E \cdot A} \right) \quad (10)$$

where:

R_{x0} : Conductor longitudinal reaction under its own weight $R_{x0} = W \cdot L_x^2 / (8S)$

E: Modulus of elasticity, A: Conductor cross section area, W: Conductor weight, S: Conductor sag

L_0 : Conductor length before the application wind loading under its own weight, which can be calculated as $L_0 = L_x \cdot \left(1 + 8/3 \cdot (S/L_x)^2 \right)$

$$L_{n+1} = \int dL_{n+1} = \int \sqrt{1 + \left(\frac{dy}{dx} \right)_{n+1}^2 + \left(\frac{dz}{dx} \right)_{n+1}^2} \cdot L_x \cdot ds \quad (11)$$

$$L_{n+1} = L_x \cdot \int_0^1 \left(1 + \frac{1}{2} \left(\frac{dy}{dx} \right)_{n+1}^2 + \frac{1}{2} \left(\frac{dz}{dx} \right)_{n+1}^2 \right) ds \tag{12}$$

$$\left(\frac{dy}{dx} \right)_{n+1} = \frac{Q_{yn+1}(s)^*}{R_{xn+1}} + \frac{(dy_{N+1} - dy_N)}{L_x} \tag{13}$$

$$\left(\frac{dz}{dx} \right)_{n+1} = \frac{Q_{zn+1}(s)^*}{R_{xn+1}} + \frac{(dz_{N+1} - dz_N)}{L_x} \tag{14}$$

$$Q_y(s)^* = \frac{M_{zgyB}}{L_x} - L_x \cdot \int_0^s g_y(s_1) \cdot ds_1 \tag{15}$$

$$Q_z(s)^* = \frac{M_{ygzB}}{L_x} - L_x \cdot \int_0^s g_z(s_1) \cdot ds_1 \tag{16}$$

$$R_{xn+1} = \sqrt{\frac{\int_0^1 Q_{yn+1}(s)^*{}^2 ds + \int_0^1 Q_{zn+1}(s)^*{}^2 ds + 2 \cdot \frac{R_{xn+1}}{L_x} \left((dy_{N+1} - dy_N) \int_0^1 Q_{yn+1}(s)^* ds + (dz_{N+1} - dz_N) \int_0^1 Q_{zn+1}(s)^* ds \right)}{2 \left(\frac{L_0}{L_x + dx_{N+1} - dx_N} \left(\frac{R_{xn+1} - R_{x0}}{EA} + 1 \right) - 1 \right)}} \tag{17}$$

$$R_{xN} = R_{xn+1} - R_{xn} = \sqrt{\frac{a_n}{\left(\frac{L_0 \cdot b_n}{L_x + dx_{N+1} - dx_N} - 1 \right)}} - \sqrt{\frac{a_{n-1}}{\left(\frac{L_0 \cdot b_{n-1}}{L_x + dx_N - dx_{N-1}} - 1 \right)}} \tag{18}$$

where

$$a_n = \frac{1}{\sqrt{2}} \sqrt{\int_0^1 Q_{yn}(s)^*{}^2 ds + \int_0^1 Q_{zn}(s)^*{}^2 ds + 2 \cdot \frac{R_{xn}}{L_x} \left((dy_{N+1} - dy_N) \int_0^1 Q_{yn}(s)^* ds + (dz_{N+1} - dz_N) \int_0^1 Q_{zn}(s)^* ds \right)}$$

$$b_n = 1 + \frac{R_{xn} - R_x}{EA}$$

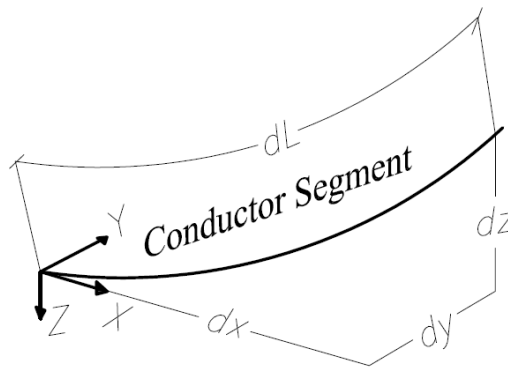


Fig. 4 Conductor segment

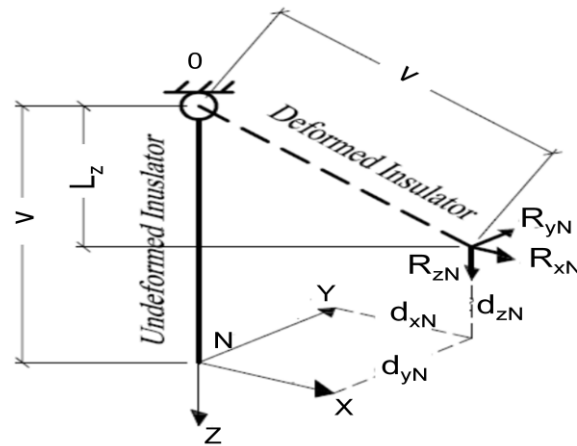


Fig. 5 The insulator equilibrium state

2.3 Insulator equilibrium

Insulators are modeled as rigid pendulums with length, v , which is constant before and after the application of the loading. Considering an insulator, N , as shown in Fig. 5, and applying the equilibrium of the moment at the hanging point, 0 , around x , y and z axes, a relationship between the nodal displacements (d_{xN} , d_{yN} and d_{zN}) and the nodal reactions (R_{xN} , R_{yN} and R_{zN}) is obtained as given by Eqs. (19)-(21). Eqs. (19)-(21), which describe the insulator response, have six unknowns: three displacement components, d_{xN} , d_{yN} and d_{zN} , and three reaction components, R_{xN} , R_{yN} and R_{zN} . Eqs. (8), (9) and (18) share the same six unknowns and describe the conductor response. Therefore, a combination of these Eqs. ((8),(9),(18), (19), (20) and (21)) can be used to solve the entire system as will be illustrated by Section 3.

$$d_{xN} = v \cdot \frac{R_{xN}}{R_{resN}} \quad (19)$$

$$d_{yN} = v \cdot \frac{R_{yN}}{R_{resN}} \quad (20)$$

$$L_{zN} = v \cdot \frac{R_{zN}}{R_{resN}} \quad (21)$$

Where:

R_{resN} :: The resultant force at node N , $R_{resN} = \sqrt{R_{xN}^2 + R_{yN}^2 + R_{zN}^2}$

L_{zn} L_{zN} : The vertical projection of the insulator after the deformation $= v + d_{zn}$, where d_{zn} is the displacement in the Z direction, which is usually negative.

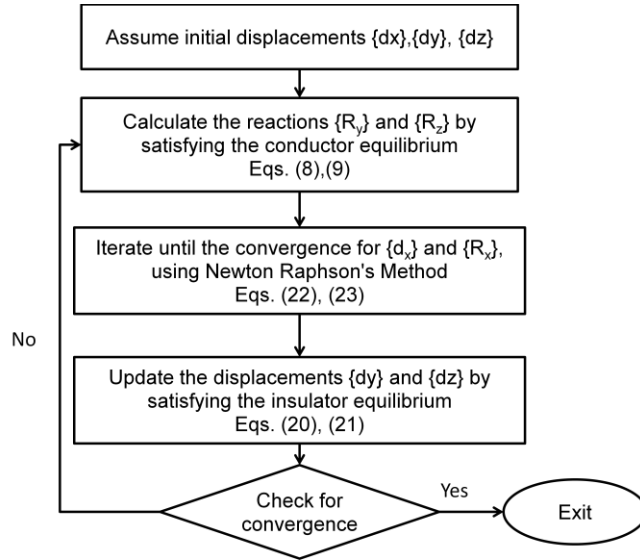


Fig. 6 Flow chart of the proposed solution approach

3. Solution technique

At each conductor-insulator connecting point, six non-linear equations exist, which are Eqs. (8), (9), (18), (19), (20) and (21), and six unknowns also exist, which are the displacement components and three reaction components. Since the number of equations equals the number of unknowns, the problem can be solved. However, such a system of equations needs to be solved iteratively. The easiest approach to solve those equations is by iterating in a sequential manner, where only one equation is solved at a time. First, initial displacements are to be assumed. Then, the reactions are to be updated using Eqs. (8), (9) and (18) to satisfy the conductor equilibrium, and then the nodal displacements are to be updated using Eqs. (19)-(21) to satisfy the insulator equilibrium until convergence takes place. It is found that such sequential techniques can be easily unstable. The instability may happen in Eq. (18), while attempting to update the reactions in x direction, R_x , assuming constant displacements in x-direction, dx . This instability is due to the high level of coupling between displacements and reactions in the x-direction. Consequently, a more stable approach, illustrated by the flow chart shown in Fig. 6, is proposed. As indicated by the flow chart, Newton Raphson's iterative method is utilized to solve Eq. (18) with Eq. (19) simultaneously in d_x and R_x while assuming the other variables as constants. The displacement vector in x direction at iteration number $i+1$, $\{d_x\}_{Ndx1}^{i+1}$, is calculated using Eq. (22) as a function of the displacement vector at the previous iteration i , $\{d_x\}_{Ndx1}^i$. After convergence takes place, the reaction vector, R_x , is calculated from the displacement vector using Eq. (23).

$$\{d_x\}_{Ndx1}^{i+1} = \{d_x\}_{Ndx1}^i + [K_x]_{NdxNd} \cdot \{f_x\}_{Ndx1}^i \tag{22}$$

Where:

i: Iteration number

$\{f_x\}_{Ndx1}$: Unbalanced load vector in, which is defined in Appendix 1

$[K_x]_{NdxNd}$: Tangential stiffness matrix that is given in Appendix 1, whose the (N, J) element equals to $-\frac{\partial f(N)}{\partial x(J)}$, where N and J are the row and the column numbers

$$R_x(N) = d_x(N) \cdot \frac{R_{res}(N)}{V} \quad (23)$$

4. Validating the technique

Two cases of loading are selected in order to validate the developed technique. The first case of loading represents a downburst, while the second represents a tornado. Downburst and tornado wind fields resulting from the CFD simulation performed by Hangan and Kim (2007) and Hangan and Kim (2008) are utilized. The technique illustrated by Shehata *et al.* (2005) is employed to scale up the CFD results and to calculate wind forces on the conductors. According to Shehata and El Damatty (2007) and Hamada and El Damatty (2011), the behaviour of a Transmission Line (TL) under HIW is strongly dependent on the event size, D, and the relative location between the event and the towers, defined by the polar coordinates, R and Θ . Values of those parameters for the considered cases of downburst and tornado are given by Figs. 7 and 8, respectively. According to El Damatty and Aboshosha (2012), Aboshosha and El Damatty (2013) and El Damatty and Hamada (2012), those parameters are found to be critical for the considered lines and can lead to the failure of the intermediate tower. Those downburst and tornado configurations induce unequal wind loads acting on the conductors located on either sides of the middle tower. The HIW parameters of the chosen events are summarized in Table 1, while the corresponding distribution of wind loads is given in Figs. 9 and 10, respectively. As shown in Figs. 9 and 10, only six conductor spans adjacent to the intermediate tower are chosen in the analysis, similar to the number used by Shehata *et al.* (2005). Shehata *et al.* (2005) showed that analyzing six spans is enough to obtain accurate prediction of the transmitted forces from the conductors to the intermediate tower. The first and last nodes of the considered six-spanned system are assumed to be restrained in the three directions, similar to the system analyzed by Shehata *et al.* (2005). The properties of the chosen conductor are summarized in Table 2.

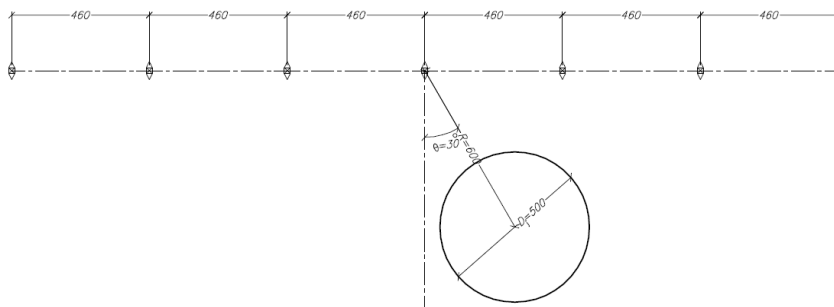


Fig. 7 Downburst loading case

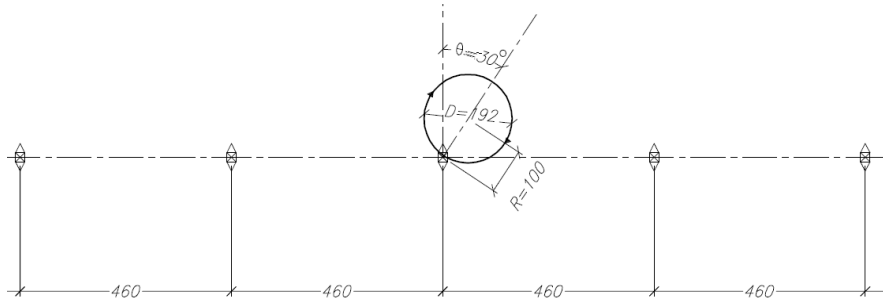


Fig. 8 Tornado loading case

Table 1 Loading parameters

Downburst Loading Parameters	Tornado Loading Parameters
D=500.0 m	D=192.0 m
R _j =600.0 m	R=100.0 m
Θ=30°	Θ=-30°
Jet Velocity, V _j =40.0 m/s	Tornado F2 on Fujita Scale, with maximum tangential velocity =78 m/s happens at 96.0 m from the tornado eye

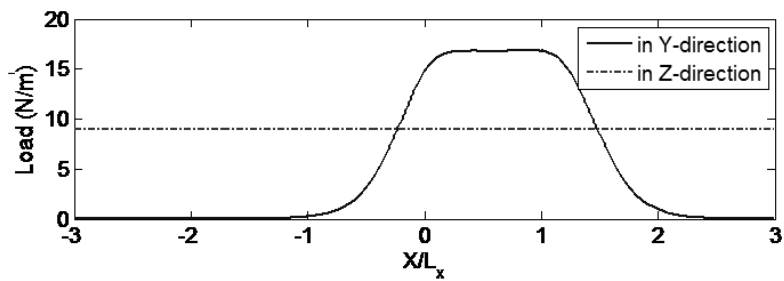


Fig. 9 Load distribution induced from the Downburst Loading

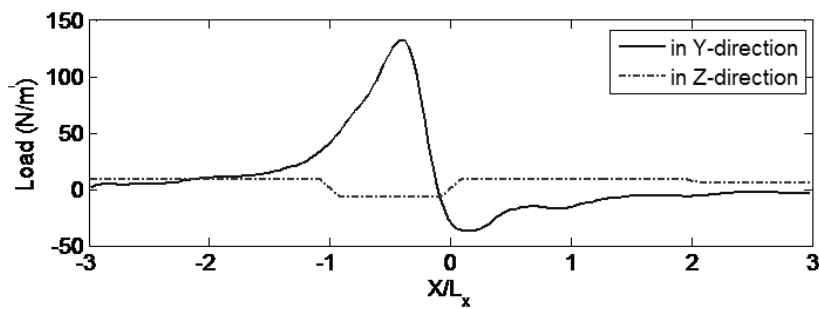


Fig. 10 Load distribution induced from the Tornado Loading

Table 2 Properties of the Conductor

Property	Value
Span Length L_x (m)	460.0
Sag Length S (m)	16.0
Elasticity Modulus E (N/m ²)	5.2E10
Weight W (N/m)	8.96
Facing Area from the wind (m ² /m)	0.022
Drag coefficient C_d	1.0
Cross sectional Area (m ²)	3.80E-04
Insulator Length v (m)	4.0
Insulator Axial Stiffness	Rigid
Elevation for the hanging point (m)	40.0

4.1 Results of the analysis

The results are obtained in terms of the nodal displacements and nodal reactions as summarized in Table 3 for the downburst case and in Table 4 for the tornado case. A deformed shape can be obtained using the expressions provided by the following Eqs.

$$dy_{n+1}(s) = dy_n + \frac{(RA_y)_{n+1} \cdot L_x \cdot s - L_x^2 \cdot \int_{s_1=0}^{s_1=s} g_y(s_1) \cdot (s - s_1) \cdot ds_1}{Rx_{n+1}} \quad (24)$$

$$dz_{n+1}(s) = dz_n + \frac{(RA_z)_{n+1} \cdot L_x \cdot s - L_x^2 \cdot \int_{s_1=0}^{s_1=s} g_z(s_1) \cdot (s - s_1) \cdot ds_1}{Rx_{n+1}} \quad (25)$$

Such expressions are based on equating the bending moments at a general location, s , inside a span, $n+1$, to zero. The obtained deformed shape is plotted in Figs. 11 and 12 for the downburst and tornado cases, respectively. In order to assess the accuracy and the efficiency of the proposed technique, the same conductor system is reanalyzed using Finite Element Analysis (FEA). The commercial software package SAP 2000 is utilized to perform the FEA, using a 3D cable element to simulate the conductors, a technique similar to what was done by Hamada and El Damatty (2011). In the SAP program, each conductor span is divided into 30 elements to account for the load variation along the length. The resulting deformed shape obtained using the FEA is plotted and compared with that from the proposed technique as shown in Figs. 11 and 12 for the downburst and the tornado cases, respectively. It is clear from the figures that the two responses are in good agreement. Nodal displacements and reactions obtained from the FEA are summarized in Tables 3 and 4 for the downburst and the tornado cases, respectively. Differences between the responses predicted using the proposed technique and those by employing the FEA are also summarized in the two tables. The maximum differences in the displacements are 3% and 5% for the downburst and the tornado cases, respectively. In the meanwhile, the maximum differences in the reactions are 4% and 6% for the downburst and the tornado cases, respectively. Such an agreement between the analytical and FEA results provides a validation for the developed technique. In terms of efficiency, the proposed technique shows a significant reduction in the

computational time required to perform the analysis, when compared with the FEA. The technique required only 0.35 seconds to solve the six-spanned problem, while FEA takes 65 seconds to solve the same problem. This means that the proposed technique is about 186 and 185 times faster than the FEA. It important to mention that a large parametric study is often required by varying the event size and location in order to obtain the maximum forces acting on a tower due to HIW event. As such the saving in the computational time of one analysis makes a large difference in the overall time required to conduct a parametric study. For example, the parametric study conducted by Shehata and El Damatty (2007), which involved 308 load cases took 44.6 hours using FEA, while it has taken only 18 minutes using the developed technique in this study.

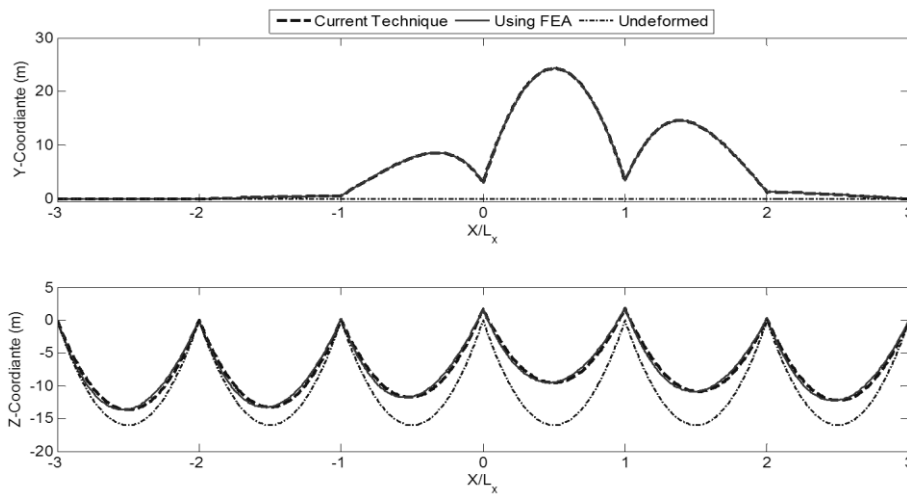


Fig. 11 Deflected shape under downburst loading

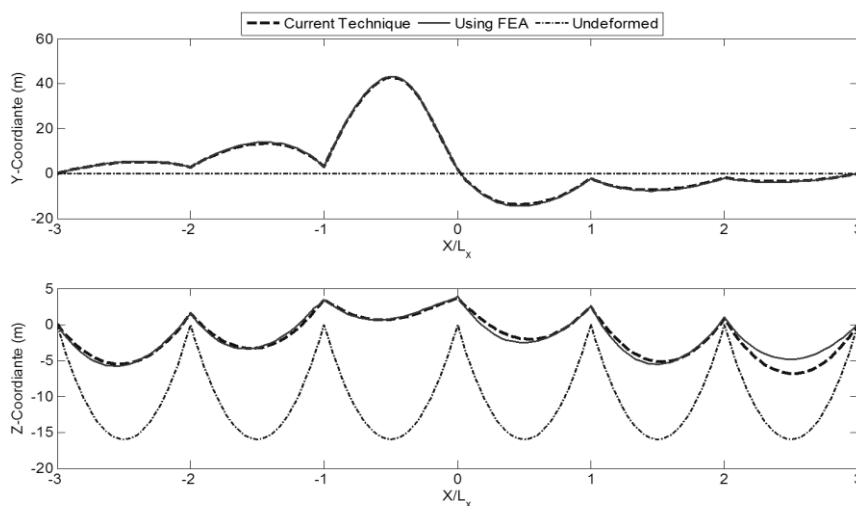


Fig. 12 Deflected shape under tornado loading

Table 3 Nodal reactions and displacement results for the downburst Case

Joint	FEA			Current Technique			Difference %		
	d_x (m)	d_y (m)	d_z (m)	d_x (m)	d_y (m)	d_z (m)	d_x	d_y	d_z (m)
2	0.412	0.027	-0.022	0.422	0.027	-0.022	2%	1%	-3%
3	0.886	0.618	-0.148	0.909	0.613	-0.153	3%	1%	-3%
4	1.210	3.021	-1.67	1.235	3.018	-1.683	2%	0%	0%
5	-0.533	3.335	-1.85	-0.548	3.333	-1.858	-3%	0%	0%
6	-0.648	1.275	-0.26	-0.668	1.268	-0.265	-3%	1%	0%

Joint	FEA			Current Technique			Difference %		
	R_x (N)	R_y (N)	R_z (N)	R_x (N)	R_y (N)	R_z (N)	R_x (N)	R_y (N)	R_z (N)
1	17356	1	2065	17313	1	2081	0%	1%	1%
2	428	28	4127	441	28	4159	3%	1%	1%
3	937	653	4074	970	654	4106	4%	0%	1%
4	2178	5438	4186	2247	5491	4217	3%	1%	1%
5	-1045	6538	4209	-1085	6596	4240	-4%	1%	1%
6	-706	1390	4073	-734	1394	4105	-4%	0%	1%
7	-19178	69	2055	-19152	69	2070	0%	0%	1%

5. Conclusions

A new technique is developed to analyze multi-spanned transmission line conductor systems under HIW. The technique divides the system at the conductor-insulator connecting points, where six unknowns appear: three reaction components and three displacement components. Six equations are required to solve for those unknowns. Three equations are derived by satisfying the moment equilibrium of the conductors and by equating the conductor length using two different approaches. The remaining three equations are derived by satisfying the moment equilibrium of the insulators. The resulting six equations are nonlinear and coupled. As such, an iterative technique is suggested to solve the governing equations. In this technique, equations that govern the longitudinal responses are solved in a coupled way while the rest of the equations are solved sequentially. The proposed technique is the first that is based on a semi-closed form solution and is able to solve for a multi-spanned conductor systems subjected to varying loads in the transverse and vertical directions, while accounting for the insulator flexibility. Accuracy and efficiency of the technique are tested under two different cases of HIW. The technique showed good agreement in terms of the predicted reactions and displacements, when compared with FEA. The maximum difference in the displacement between the two methods is 4% for the downburst and 5% for the tornado cases. In terms of the reactions, a maximum difference of 5% for the downburst case and of 6% for the tornado case is found. The method shows a significant reduction in the

computational time compared to FEA. The technique is shown to be 185 times faster than the FEA, for the considered cases. Analysis of transmission lines under HIW requires conducting a large number of analyses to capture the potential sizes and locations of these localized events. As such, a reduction in the computational time for each analysis becomes very important and useful for this type of application.

Acknowledgments

The authors would like to thank the National Research Council of Canada (NSERC), Hydro One Company and the Ontario Centre of Excellence (OCE) for their kind financial support of this research.

References

- Aboshosha, H. and El Damatty, A. (2013), "Downburst induced forces on the conductors of electric transmission lines and the corresponding vulnerability of tower failure", *Proceedings of the Canadian Society of Civil Engineers CSCE 2013, Montreal, Québec, Canada-GEN-164*.
- Ahmadi-Kashani, K. and Bell, A.J. (1988), "The analysis of cables subject to uniformly distributed loads", *Eng. Struct.*, **10**(3), 174-184.
- Darwish M., El Damatty A. and Hangan, H. (2010), "Dynamic characteristics of transmission line conductors and behaviour under turbulent downburst loading", *Wind Struct.*, **13**(4), 327-346.
- El Damatty, A. and Hamada, A. (2012), "Behaviour of guyed transmission line structures under tornado wind loads – case studies", *Proceedings of the ASCE -Structural Engineering Institute – Electrical Transmission and Substation Structures Conference*, Columbus, Ohio, USA, November .
- El Damatty, A. and Aboshosha, H. (2012), "Capacity of electrical transmission towers under downburst loading", *Proceedings of the 1st Australasia and South-East Asia Structural Engineering and Construction Conference*, Perth, Australia.
- Fujita, T.T. (1990), "Downbursts: meteorological features and wind field characteristics", *J. Wind Eng. Ind. Aerod.*, **36**(1), 75-86.
- Hangan, H. and Kim, J. (2007), "Numerical simulations of impinging jets with application to downbursts", *J. Wind Eng. Ind. Aerod.*, **95**(4), 279-298.
- Hangan, H. and Kim, J. (2008), "Swirl ratio effects on tornado vortices in relation to the Fujita scale", *Wind Struct.*, **11**(4), 291-302.
- Hamada, A. and El Damatty, A.A. (2011), "Behaviour of guyed transmission line structures under tornado wind loading", *Comput. Struct.*, **89**(11-12), 986-1003.
- Irvine, H.M. (1981), *Cable structures*, MIT Press, Cambridge.
- Koziey, B. and Mirza, F. (1994), "Consistent curved beam element", *Comput. Struct.*, **51**(6), 643-654.
- Li, C.Q. (2000), "A stochastic model of severe thunderstorms for transmission line design", *Probabilist. Eng. Mech.*, **15**, 359-364.
- Manitoba Hydro Transmission and Civil Design Department (1999), "Bipole 1 & 2 HVDC transmission line wind storm failure on September 5, 1996 review of emergency response, restoration and design of these lines", Manitoba Hydro, 98-L1/1-37010-06000, 54.
- Savory, E., Parke, G.A.R., Zeinoddini, M., Toy, N. and Disney, P. (2001), "Modeling of tornado and microburst-induced wind loading and failure of a lattice transmission tower", *Eng. Struct.*, **23**(4), 365-375.
- Shehata, A.Y., El Damatty, A.A. and Savory, E. (2005), "Finite element modeling of transmission line under downburst wind loading", *Finite Elem. Anal. Des.*, **42**(1), 71-89.

- Shehata, A.Y. and El Damatty, A.A. (2007), "Behaviour of guyed transmission line structures under downburst wind loading", *Wind Struct.*, **10**(3), 249-268.
- Shehata, A.Y. and El Damatty, A.A. (2008), "Failure analysis of a transmission tower during a microburst", *Wind Struct.*, **11**(3), 193-208.
- Wei, P., Bingnan, S. and Jinchun T. (1999), "A catenary element for the analysis of cable structures", *Appl. Math. Mech. Eng.*, **20**(5), 0253-4827
- Winkelman, P.F. (1959), "Sag-tension computations and field measurements of Bonneville power administration", *AIEE Paper*, 59-900
- Yu, P., Wong, P. and Kaempffer, F. (1995), "Tension of conductor under concentrated loads", *J. Appl. Mech. - T. ASME*, **62**(3), 802-809.

JH

Appendix 1

Definition for the reaction vectors $\{R_y^F\}$ and $\{R_z^F\}$ and for the matrix $[K]_{Nd \times Nd}$

$$\{R_y^F\} = \left\{ \begin{array}{c} \frac{M_{zgyA \ 1}}{L_x} \\ \frac{M_{zgyB \ 1} + M_{zgyA \ 2}}{L_x} \\ \frac{M_{zgyB \ 2} + M_{zgyA \ 3}}{L_x} \\ \vdots \\ \frac{M_{zgyB \ Nd-2} + M_{zgyA \ Nd-1}}{L_x} \\ \frac{M_{zgyB \ Nd-1}}{L_x} \end{array} \right\}, \quad \{R_z^F\} = \left\{ \begin{array}{c} \frac{M_{ygzA \ 1}}{L_x} \\ \frac{M_{ygzB \ 1} + M_{ygzA \ 2}}{L_x} \\ \frac{M_{ygzB \ 2} + M_{ygzA \ 3}}{L_x} \\ \vdots \\ \frac{M_{ygzB \ Nd-2} + M_{ygzA \ Nd-1}}{L_x} \\ \frac{M_{ygzB \ Nd-1}}{L_x} \end{array} \right\}$$

$$[K]_{Nd \times Nd} = \left[\begin{array}{cccccc} \frac{R_{x1}}{L_x} & -\frac{R_{x1}}{L_x} & 0 & 0 & \dots & 0 \\ -\frac{R_{x1}}{L_x} & \frac{R_{x1}}{L_x} + \frac{R_x}{L_x} & -\frac{R_{x2}}{L_x} & 0 & \dots & 0 \\ 0 & -\frac{R_{x2}}{L_x} & \frac{R_{x2}}{L_x} + \frac{R_x}{L_x} & -\frac{R_{x3}}{L_x} & \dots & 0 \\ \vdots & \vdots & \vdots & \vdots & \ddots & \vdots \\ 0 & 0 & 0 & -\frac{R_{xNd-2}}{L_x} & \frac{R_{xNd-2}}{L_x} + \frac{R_{xNd-1}}{L_x} & -\frac{R_{xNd-1}}{L_x} \\ 0 & 0 & 0 & 0 & -\frac{R_{xNd-1}}{L_x} & \frac{R_{xNd-1}}{L_x} \end{array} \right]$$

Where:

M_{igK} : The first order moment around i axis at point K induced by a loading $g_j(s)$

L_x : Span Length

Definition for the unbalanced load vector, $\{f_x\}_{Ndx1}$, and the tangential stiffness matrix, $[K_x]_{NdxNd}$, in x-direction

$$\{f_x\}_{Ndx1} = \begin{Bmatrix} R_{x1} - d_{x1} \frac{R_{res1}}{V} \\ R_{x2} - R_{x1} - d_{x2} \frac{R_{res2}}{V} \\ \vdots \\ R_{xNd-1} - R_{xNd-2} - d_{xNd-1} \frac{R_{resNd-1}}{V} \\ R_{xNd-1} - d_{xNd} \frac{R_{resNd}}{V} \end{Bmatrix}$$

$$[K_x]_{NdxNd} = \begin{bmatrix} \frac{R_{res1}}{V} + C_1 & -C_1 & 0 & 0 & \dots & 0 \\ -C_1 & C_1 + \frac{R_{res2}}{V} + C_2 & -C_2 & 0 & \dots & 0 \\ 0 & -C_2 & C_2 + \frac{R_{res3}}{V} + C_3 & -C_3 & \dots & 0 \\ \vdots & \vdots & \vdots & \ddots & \vdots & \vdots \\ 0 & 0 & \dots & -C_{Nd-2} & C_{Nd-2} + \frac{R_{resNd-1}}{V} + C_{Nd-1} & -C_{Nd-1} \\ 0 & 0 & \dots & 0 & -C_{Nd-1} & C_{Nd-1} + \frac{R_{resNd}}{V} \end{bmatrix}$$

Where

$$C_n = \frac{L_0 \cdot b_n \cdot a_n}{2(L_x + dx_{N+1} - dx_N)^2 \cdot \left(\frac{L_0 \cdot b_n}{L_x + dx_{N+1} - dx_N} - 1\right)^{3/2}}$$